*minerals*

*Article*

# Geochemistry and Mineralogy of Lower Paleozoic Heituao Shale from Tadong Low Uplift of Tarim Basin, China: Implication for Shale Gas Development

**Shihu Zhao [1], Yanbin Wang [1], Yong Li [1,*], Honghui Li [2], Zhaohui Xu [2] and Xun Gong [1]**

1 School of Geoscience and Surveying Engineering, China University of Mining and Technology, Beijing 100083, China; tsp150201042@student.cumtb.edu.cn (S.Z.); wyb@cumtb.edu.cn (Y.W.); 1510280105@student.cumtb.edu.cn (X.G.)
2 Research Institute of Petroleum Exploration and Development, Beijing 100083, China; lhh@petrochina.com.cn (H.L.); zhaohui.xu@petrochina.com.cn (Z.X.)
* Correspondence: liyong@cumtb.edu.cn; Tel.: +86-159-0101-9002

**Abstract:** Tarim Basin is the largest Petroliferous basin in China, while its shale gas development potential has not been fully revealed. The organic-rich black shale in middle Ordovician Heituao Formation from Tadong low uplift of Tarim Basin has been considered as an important source rock and has the characteristic of large thickness, high organic matter content and high thermal maturity degree. To obtain its development potential, geochemical, mineralogical and mechanics research is conducted based on Rock-Eval pyrolysis, total organic carbon (TOC), X-ray diffraction (XRD) and uniaxial compression experiments. The results show that: (1) the TOC content ranges between 0.63 and 2.51 wt% with an average value of 1.22 wt%, the Tmax values are 382–523 °C (average = 468.9 °C), and the S2 value is relatively low which ranges from 0.08 to 1.37 mg HC/g rock (averaging of 0.42 mg HC/g rock); (2) the organic matter of Heituao shale in Tadong low uplift show poor abundance as indicated by low S2 value, gas-prone property, and post mature stage (stage of dry gas). (3) Quartz is the main mineral component in Heituao shale samples, accounting for 26–94 wt% with an average of 72 wt%. Additionally, its Young's modulus ranges from 20.0 to 23.1 GPa with an average of 21.2 GPa, Poisson's ratio ranges between 0.11 and 0.21 (average = 0.15); (4) the fracability parameter of brittleness index (BI) ranges between 0.28 and 0.99 (averaging of 0.85), indicating good fracability potential of Heituao shale of Tadong low uplift and has the potential for shale gas development. This study reveals the shale gas accumulation potential in middle Ordovician of the Tarim Basin, and beneficial for future exploration and production practice.

**Keywords:** Rock-Eval pyrolysis; total organic carbon; thermal maturity; fracability evaluation



**Citation:** Zhao, S.; Wang, Y.; Li, Y.; Li, H.; Xu, Z.; Gong, X. Geochemistry and Mineralogy of Lower Paleozoic Heituao Shale from Tadong Low Uplift of Tarim Basin, China: Implication for Shale Gas Development. *Minerals* **2021**, *11*, 635. https://doi.org/10.3390/min11060635

Academic Editor: Stephen E Laubach

Received: 16 April 2021
Accepted: 12 June 2021
Published: 15 June 2021



## 1. Introduction

Shale gas is a kind of unconventional natural gas existing in the reservoir rock mainly organic-rich shale with the characteristics of clean and efficient [1,2]. The breakthrough of shale gas exploration in North America has made research on shale gas increase all over the world [3–5]. With the successful commercial development of shale gas in Sichuan Basin [6,7], scholars have been studying its accumulation and exploitation mode and looked for the possibility of shale gas development in other basins of China [8–10]. Tarim Basin is the largest Petroliferous basin in China, while its shale gas development potential has not been fully revealed [11,12]. The organic-rich black shale in Heituao Formation of middle Ordovician in Tarim Basin has been considered as an important source rock in the field of conventional oil and gas exploration [13,14], and that in Tadong low uplift is characterized by large thickness, high content of organic matter and high degree of thermal maturity [15]. In addition, Heituao shale in Tadong low uplift shows similar geological conditions and geochemical characteristics with Wufeng Formation shale in

Sichuan Basin [16,17], which suggests the potential of shale gas exploration in this area. Therefore, it is very important to carry out good research on Heituao shale to provide theoretical guidance for shale gas exploration and development in Tadong low uplift. As a key factor affecting shale gas accumulation, total organic carbon (TOC) content not only determines the amount of hydrocarbon generation, but also provides important storage space for oil and gas formation [1,18,19]. In addition, the mineral composition determines the fracability effect of shale reservoir, which is an important influencing factor of shale gas development [20,21]. However, there are few studies on the organic geochemistry and mineral composition of Heituao shale in Tadong low uplift, and the understanding of the area is insufficient [13–15].

Therefore, this study takes the middle Ordovician Heituao shale in the study area as the research object, carries out organic geochemical, mineralogical and mechanics studies, aiming to reveal its organic geochemical, mineralogical and mechanical characteristics, and clarify the main control factors of shale gas development in the area. The above studies are beneficial for future exploration and production practice in the study area.

## 2. Geological Setting

The Tarim basin is a superimposed composite basin with rich oil and gas resources in western China (Figure 1a), which are divided into seven tectonic units (three uplifts and four depressions, i.e., North Tarim uplift, Central uplift, Southeast uplift, Kuqa depression, North Tarim depression, Southwest depression and Southeast depression) according to its structural features [22,23]. The uplift and its slope belt are rich in oil and gas resources, which is an important target for oil and gas exploration in Tarim Basin [15,24]. The Tadong low uplift is a secondary positive tectonic unit located in the east of the Central uplift, which is adjacent to the North Tarim depression in the north, the Southeast uplift in the south, and the Tazhong local uplift in the west. It is occupied by a NWW inclined slope belt with a small dip angle of 1~5° (Figure 1b).

The Tadong low uplift has experienced multistage tectonic movements [25–27]. During the early Sinian period, the Tarim block was formed, where rifting was weak and depositions were received only at the edge of the basin [25]. At the end of the early Ordovician, the Tadong low uplift began to form with the collision of Tarim block and the Central Kunlun-Qiangtang block in the south, and the thick overburden basin sandstones and mudstones deposited rapidly in the middle and upper Ordovician [26]. During the period from Silurian to early Triassic, the study area was uplifted and eroded in different degrees many times, after which the Tadong low uplift is basically formed. From the Late Triassic period, the study area became an intracontinental basin sandwiched by two orogenic belts from the north and south [27]. From the Paleogene period, the northern part of the basin uplifted and the sedimentary center moved southward, thus forming the present tectonic features.

The strata exposed by drilling of Tadong low uplift from top to bottom are Cenozoic Quaternary, Neogene and Paleogene; Mesozoic Cretaceous and Jurassic; Paleozoic Ordovician and Cambrian. Shale in the area is mainly distributed in the lower Cambrian mohershan Formation and Xidashan-Xishanbulake Formation, middle Ordovician Heituao Formation and upper Ordovician quekerke Formation. Among them, the Heituao shale (Figures 1c and 2) is characterized by large depth (4100–5100 m), large thickness (50–200 m), wide and stable distribution in the study area, which has good shale gas generation conditions [24].

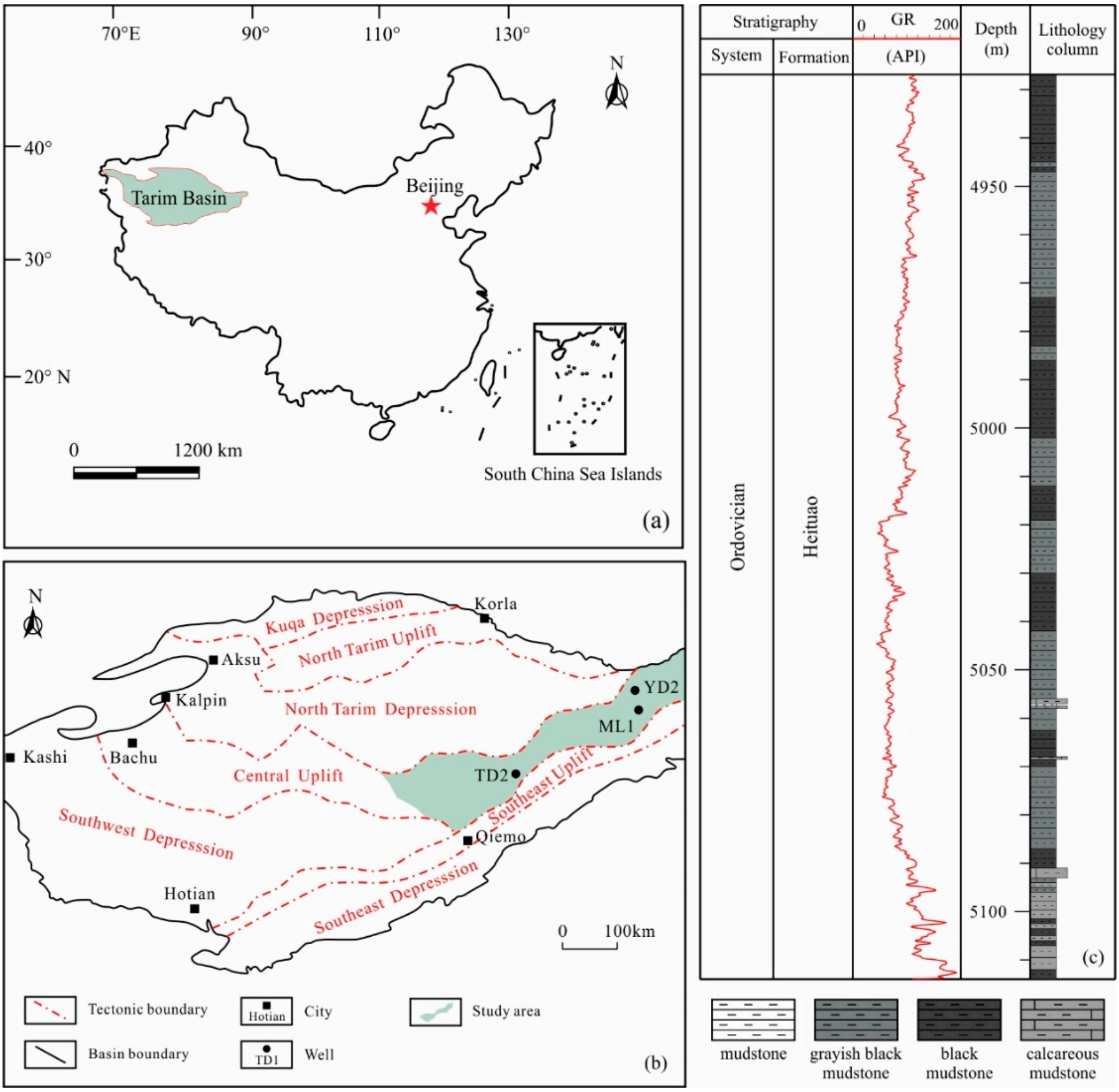


**Figure 1.** Geological overview of the Tarim Basin and of the study area: (**a**) the location of the Tarim Basin [13]; (**b**) tectonic units of the Tarim Basin and location of the study area [13]; (**c**) stratigraphic column of the Ordovician Heituao formation in the Tadong low uplift. Where GR stands for the natural gamma ray logging and API is the unit of GR.

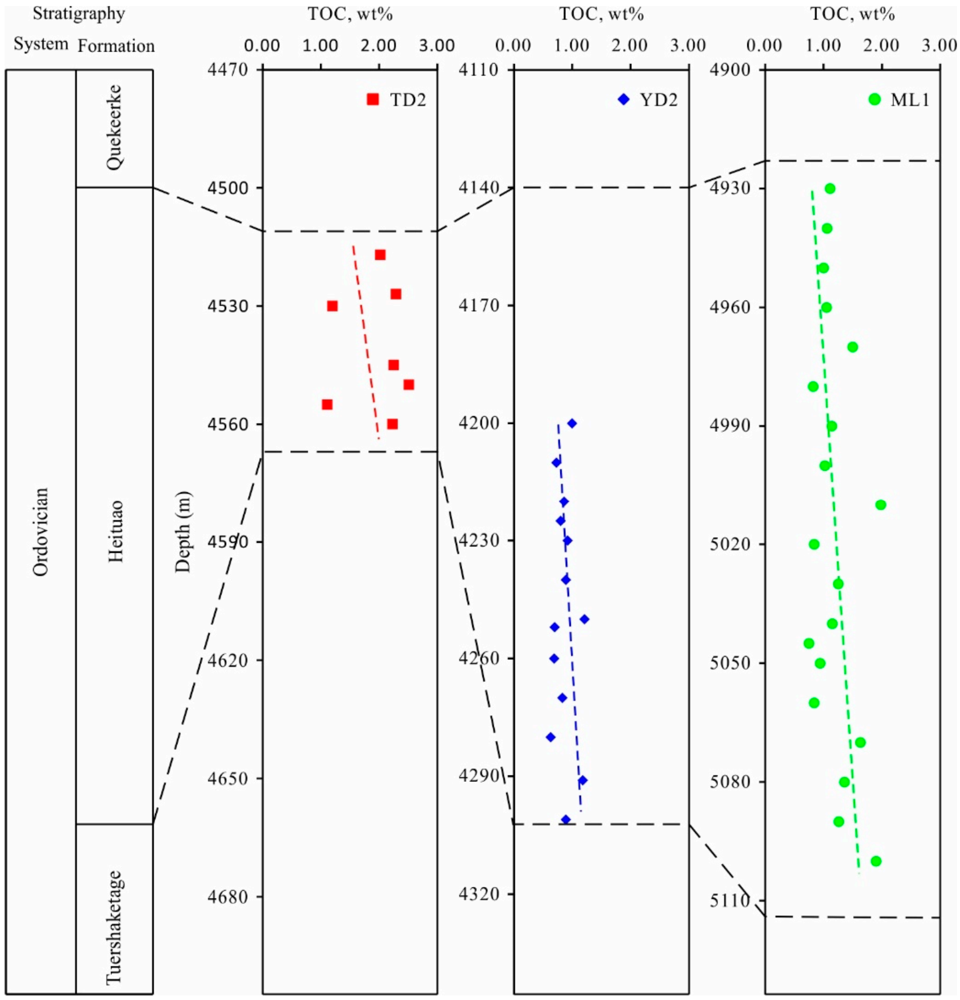


**Figure 2.** Vertical trends of the TOC content of different wells (TD2, YD2, and ML1) from Heituao shale samples in Tadong low uplift.

## 3. Materials and Methods

A total of 45 shale samples were collected from Heituao Formation in wells TD2, ML1 and YD2 of the Tadong low uplift (Figure 1c). All the shale samples were numbered consecutively from wells TD2 (sample TD2-1 to TD2-7), ML1 (sample ML1-1 to ML1-19) and YD2 (sample YD2-1 to YD2-19) with depth.

After the hydrochloric acid solution, shale samples were crushed to powders (~180 mesh), and a CS744 carbon/sulfur analyzer was used based on the Chinese National standards GB/T19145-2003 to measure the total organic carbon (TOC) contents of shale samples. The Rock-Eval pyrolysis was performed on shale powders (~180 mesh) using a YQ-VIIA (Haicheng Petrochemical Instrument Company, Anshan, China) rock pyrometer mainly to obtain the geochemical parameters of shale samples. The samples were pyrolyzed up to 540 °C for 2 h, following the Chinese National standards GB/T 18602-2012. Thus, pyrometer parameters of soluble hydrocarbon content (S1), pyrolytic hydrocarbon content (S2), pyrolysis temperature (Tmax) corresponding to the generated maximum hydrocarbon, production index (PI) and hydrogen index (HI) were characterized.

The X-ray diffraction experiment was performed on shale powders (~120 mesh) using a D/max-2200 (Rigaku, Tokyo, Japan) X-ray diffractometer at 40 kV and 40 mA with a Cu radiation to determine the mineral contents of shale samples. The scanning speed and frequency was 2°/min and 0.02° (2θ), respectively, over a long angular range (5–80° 2θ). The quantitation for the mineral composition was carried out based on the curve area of the major peaks.

The porosity and permeability tests were undertaken on shale core samples (~ϕ 25 mm × 50 mm) based on the Chinese Industry standard SY/T 5336-1996 and using a DZSY-002 (Haian Petroleum Instrument Company, Nantong, China) rock permeability tester to obtain the porosity and permeability of shale samples. Then, the shale core samples were reused to perform the uniaxial compression experiment with a servo universal testing machine to obtain the Young's modulus and Poisson's ratio of shale samples. Both end faces of the samples were smoothed with abrasive papers (roughness less than ±0.05 mm) and were perpendicular to the sample axis (discrepancy less than ±0.25°). The axial displacement rates were 0.05 and 0.1 mm/min, respectively, to control axial load increase in the pre-failure stage and after exceeding the peak strength, respectively.

## 4. Results

### 4.1. Geochemistry

The geochemical results of 45 shale samples of the Heituao Formation are shown in Table 1, including the total organic carbon (TOC), soluble hydrocarbon content (S1), pyrolytic hydrocarbon content (S2), pyrolysis temperature (Tmax), production index (PI), and hydrogen index (HI).

**Table 1.** The geochemical results of Heituao shale samples in the Tadong low uplift.

| Sample No. | Well No. | Depth (m) | TOC (%) | Tmax (°C) | S1 (mg/g) | S2 (mg/g) | PI (mg/g) | HI (mg/g) |
|---|---|---|---|---|---|---|---|---|
| ML1-1 | ML1 | 4930 | 1.11 | 437 | 0.37 | 0.36 | 0.51 | 32.53 |
| ML1-2 | ML1 | 4940 | 1.06 | 500 | 0.19 | 0.33 | 0.37 | 31.19 |
| ML1-3 | ML1 | 4950 | 1.00 | 512 | 0.14 | 0.27 | 0.34 | 27.13 |
| ML1-4 | ML1 | 4960 | 1.05 | 503 | 0.16 | 0.32 | 0.33 | 30.34 |
| ML1-5 | ML1 | 4970 | 1.50 | 506 | 0.18 | 0.39 | 0.32 | 26.08 |
| ML1-6 | ML1 | 4980 | 0.82 | 506 | 0.17 | 0.35 | 0.33 | 42.52 |
| ML1-7 | ML1 | 4990 | 1.14 | 504 | 0.15 | 0.40 | 0.27 | 34.98 |
| ML1-8 | ML1 | 5000 | 1.02 | 509 | 0.11 | 0.38 | 0.22 | 37.19 |
| ML1-9 | ML1 | 5010 | 1.98 | 500 | 0.15 | 0.48 | 0.24 | 24.21 |
| ML1-10 | ML1 | 5020 | 0.84 | 506 | 0.08 | 0.26 | 0.24 | 31.02 |
| ML1-11 | ML1 | 5030 | 1.25 | 516 | 0.09 | 0.31 | 0.23 | 24.90 |
| ML1-12 | ML1 | 5040 | 1.15 | 523 | 0.05 | 0.20 | 0.20 | 17.41 |
| ML1-13 | ML1 | 5045 | 0.75 | 513 | 0.09 | 0.08 | 0.51 | 11.00 |
| ML1-14 | ML1 | 5050 | 0.94 | 522 | 0.03 | 0.14 | 0.18 | 14.83 |
| ML1-15 | ML1 | 5060 | 0.84 | 517 | 0.06 | 0.17 | 0.26 | 20.33 |
| ML1-16 | ML1 | 5070 | 1.63 | 492 | 0.06 | 0.20 | 0.23 | 12.25 |
| ML1-17 | ML1 | 5080 | 1.36 | 508 | 0.07 | 0.22 | 0.24 | 16.15 |
| ML1-18 | ML1 | 5090 | 1.26 | 500 | 0.06 | 0.27 | 0.18 | 21.35 |
| ML1-19 | ML1 | 5100 | 1.90 | 498 | 0.07 | 0.38 | 0.16 | 20.04 |
| TD2-1 | TD2 | 4517 | 2.02 | 411 | 0.23 | 0.20 | 0.53 | 9.89 |
| TD2-2 | TD2 | 4527 | 2.29 | 419 | 0.08 | 0.08 | 0.50 | 3.00 |
| TD2-3 | TD2 | 4530 | 1.20 | 421 | 0.11 | 0.13 | 0.47 | 10.71 |
| TD2-4 | TD2 | 4545 | 2.25 | 429 | 0.25 | 0.33 | 0.44 | 14.52 |
| TD2-5 | TD2 | 4550 | 2.51 | 447 | 0.56 | 0.50 | 0.53 | 14.26 |
| TD2-6 | TD2 | 4555 | 1.11 | 425 | 0.26 | 0.25 | 0.51 | 23.00 |
| TD2-7 | TD2 | 4560 | 2.23 | 442 | 1.07 | 1.11 | 0.49 | 49.67 |
| YD2-7 | YD2 | 4200 | 1.00 | 399 | 0.62 | 0.96 | 0.39 | 96.18 |
| YD2-8 | YD2 | 4210 | 0.73 | 399 | 0.63 | 0.94 | 0.40 | 129.60 |
| YD2-9 | YD2 | 4220 | 0.86 | 382 | 0.75 | 0.95 | 0.44 | 110.84 |
| YD2-10 | YD2 | 4225 | 0.8 | 487 | 0.24 | 0.62 | 0.28 | 78.00 |
| YD2-11 | YD2 | 4230 | 0.92 | 416 | 0.81 | 1.37 | 0.37 | 148.44 |
| YD2-12 | YD2 | 4240 | 0.89 | 475 | 0.19 | 0.24 | 0.43 | 27.47 |
| YD2-13 | YD2 | 4250 | 1.21 | 444 | 0.38 | 0.45 | 0.46 | 37.04 |
| YD2-14 | YD2 | 4252 | 0.7 | 456 | 0.27 | 0.35 | 0.44 | 50.00 |
| YD2-15 | YD2 | 4260 | 0.69 | 387 | 0.30 | 0.28 | 0.52 | 40.63 |
| YD2-16 | YD2 | 4270 | 0.83 | 403 | 0.21 | 0.21 | 0.50 | 25.18 |
| YD2-17 | YD2 | 4280 | 0.63 | 488 | 0.18 | 0.25 | 0.42 | 39.51 |
| YD2-18 | YD2 | 4291 | 1.18 | 467 | 0.52 | 0.84 | 0.38 | 71.31 |
| YD2-19 | YD2 | 4301 | 0.89 | 479 | 0.25 | 0.63 | 0.28 | 71.00 |

Note: TOC, Tmax, S1, S2, PI and HI stand for total organic carbon content, soluble hydrocarbon content, pyrolytic hydrocarbon content, pyrolysis temperature corresponding to the generated maximum hydrocarbon, production index, and hydrogen index, respectively.

The TOC content of Heituao shale ranges between 0.63 and 2.51 wt% with an average of 1.22 wt%, that in well TD2 ranges from 1.11 to 2.51 wt% with an average of 1.94 wt%, that in well ML1 is between 0.75 and 1.90 wt% (average = 1.19 wt%), and that in well YD2 is between 0.63 and 1.21 wt% (average = 0.87 wt%). In addition, Figure 2 shows that almost all TOC contents of the Heituao shale in well TD2 are higher than 1 wt%, and the TOC contents in these three wells trend to increase with the increase of depth. Moreover, the TOC contents of the Heituao shale gradually decrease northeastward according to the relative position of the well in Figure 1b.

The Tmax values of Heituao shale range from 382 to 523 °C (average = 468.9 °C), showing great variation between different wells. The Tmax values in well ML1 are the highest, ranging between 477 and 523 °C with an average of 506 °C, followed by well YD2 (ranges from 382 to 488 °C, with an average of 437 °C), and well TD2 is lowest, the Tmax values of which are between 411 and 447 °C with an average of 428 °C. In addition, it can be seen from Figure 3 that the greater the depth, the higher the Tmax value of Heituao shale.

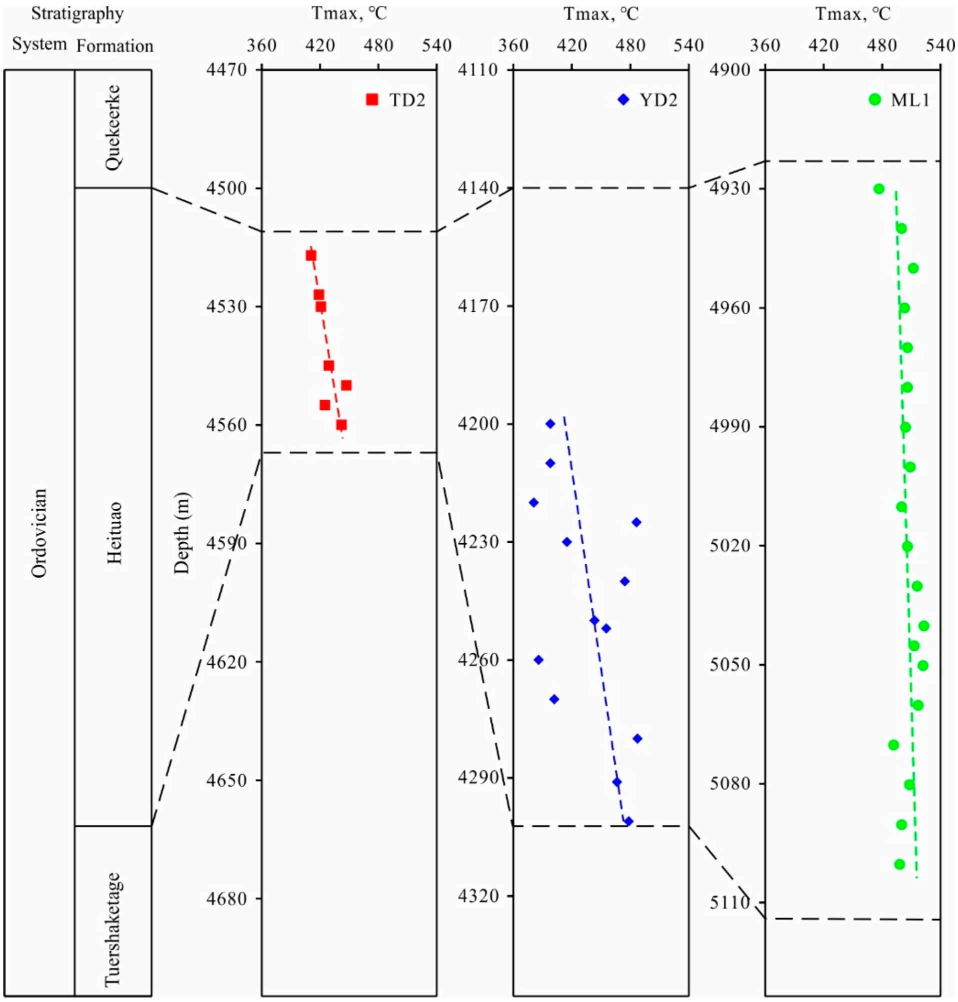


**Figure 3.** Vertical trends of the Tmax content of different wells (TD2, YD2, and ML1) from Heituao shale samples in Tadong low uplift.

The S2 value of Heituao shale is relatively low, which ranges from 0.08 to 1.37 mg HC/g rock (average = 0.42 mg HC/g rock), indicating its current hydrocarbon generation potential is low. Moreover, with the increase of depth, the variation of the S2 value is similar between ML1 and YD2 wells: increase first, then decrease and then increase (Figure 4).

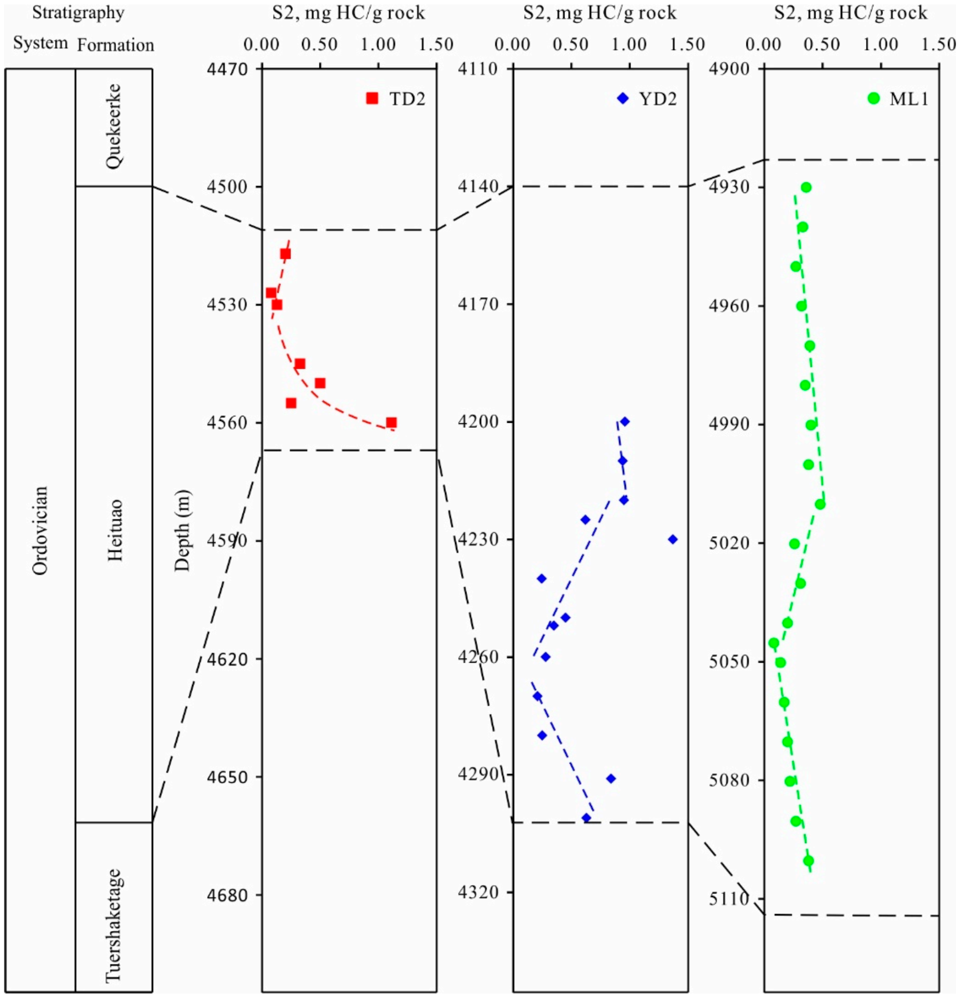


**Figure 4.** Vertical trends of the S2 content of different wells (TD2, YD2, and ML1) from Heituao shale samples in Tadong low uplift.

### 4.2. Mineralogy

The XRD experiments were conducted on 15 Heituao shale samples to determine the mineral composition, which shows that minerals in shale samples are strongly heterogeneous and quartz, clay minerals, carbonates (the sum of calcite, dolomite, ankerite, siderite and magnesite), pyrite and feldspar (including potassium feldspar and plagioclase) are dominant (Table 2). The quartz content ranges from 26 to 94 wt% with an average of 72 wt%, the clay content ranges from 0 to 66 wt% with an average of 9 wt%. The content of carbonate content ranges from 0 to 39 wt% (average = 8 wt%), that of feldspar ranges from 0 to 18 wt% (average = 6 wt%), and that of pyrite is between 0 and 19 wt% (average = 5 wt%). Abundance of pyrite indicates a euxinic sedimentary environment, which corresponds to the sedimentary indicator based on the carbon isotope parameters [28].

In addition, a ternary diagram [29] was used to plot the mineral composition of Heituao shale, where the total contents of quartz, feldspar and mica (QFM), of calcite, dolomite, ankerite, siderite and magnesite (Carbonates), and of kaolinite, illite, chlorite and montmorillonite (Clays) are equal to 100%. The result (Figure 5) shows that Heituao shale in the study area is relatively rich in quartz-feldspar-mica minerals and very poor in carbonates and clay minerals, belonging to the silica-dominated lithotype. This mineral composition may result from the burial diagenesis [30] and is very suitable for hydraulic fracturing owing to the existence of a large number of brittle minerals [31].

**Table 2.** Mineral composition and brittleness parameters of Heituao shale in the study area.

| Sample No. | Depth (m) | Minerals (%) | | | | | BI | BM |
|---|---|---|---|---|---|---|---|---|
| | | Quartz | Feldspar | Carbonate | Pyrite | Total Clays | | |
| ML1-4 | 4960 | 85 | 0 | 4 | 11 | 0 | 0.94 | 0.71 |
| ML1-7 | 4990 | 91 | 8 | 0 | 0 | 1 | 0.98 | 0.71 |
| ML1-12 | 5040 | 79 | 6 | 0 | 14 | 1 | 0.98 | 0.71 |
| ML1-16 | 5070 | 88 | 4 | 0 | 7 | 1 | 0.98 | 0.71 |
| ML1-19 | 5100 | 94 | 0 | 3 | 3 | 0 | 0.95 | 0.71 |
| YD2-3 | 4160 | 60 | 0 | 37 | 3 | 0 | 0.99 | 0.83 |
| YD2-6 | 4190 | 81 | 0 | 8 | 2 | 9 | 0.91 | 0.72 |
| YD2-9 | 4220 | 79 | 0 | 15 | 6 | 0 | 0.83 | 0.71 |
| YD2-13 | 4250 | 75 | 0 | 6 | 19 | 0 | 0.91 | 0.71 |
| YD2-17 | 4280 | 26 | 5 | 0 | 3 | 66 | 0.28 | 0.26 |
| TD2-1 | 4517 | 88 | 10 | 0 | 0 | 2 | 0.96 | 0.69 |
| TD2-3 | 4530 | 70 | 15 | 6 | 9 | 0 | 0.98 | 0.73 |
| TD2-4 | 4545 | 37 | 17 | 0 | 0 | 46 | 0.43 | 0.35 |
| TD2-6 | 4555 | 89 | 0 | 8 | 0 | 3 | 0.96 | 0.72 |
| TD2-7 | 4560 | 42 | 18 | 39 | 0 | 1 | 0.69 | 0.75 |

Note: BI and BM stand for the brittleness index and brittleness of minerals, respectively, both showing the fracability of shale samples.

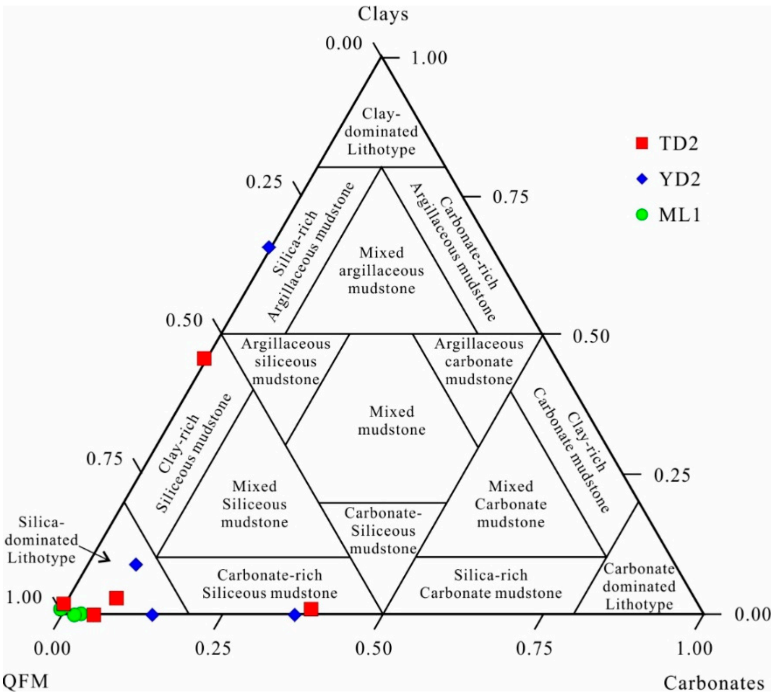


**Figure 5.** The lithotype classification based on ternary diagram of mineralogical composition from Heituao shale samples in Tadong low uplift. Modified after Glaser et al., 2014 [29].

## *4.3. Porosity and Permeability*

Limited by the coring samples, four shale core columns were used to carry out porosity and permeability tests. The results (Table 3) show that the porosity of the Heituao shale in the study area ranges from 0.067% to 1.304% with an average of 0.404%, and the Permeability ranges between 0.0010 and 0.0026 mD with an average of 0.0016 mD. The above results suggest that Heituao shale has the characteristics of ultra-low porosity and permeability, which purport the necessity to transform the shale reservoir by means of hydraulic fracturing before shale gas exploitation.

**Table 3.** Porosity and permeability of Heituao shale in the Tadong low uplift.

| Sample No. | Depth (m) | Diameter (mm) | Height (mm) | Weight (g) | Porosity (%) | Permeability (mD) |
|---|---|---|---|---|---|---|
| ML1-7 | 4990 | 25 | 55.3 | 72.8 | 0.144 | 0.0014 |
| TD2-3 | 4530 | 25 | 55.64 | 59.4 | 0.067 | 0.0012 |
| TD2-4 | 4545 | 25 | 45.7 | 73.6 | 0.102 | 0.0010 |
| TD2-6 | 4555 | 25 | 36.12 | 50.4 | 1.304 | 0.0026 |

### *4.4. Rock Mechanics*

Followed by porosity and permeability test, four shale core columns were used to carry out uniaxial compression experiments [32]. The results (Table 4) show that the Young's modulus of the Heituao shale in the study area ranges from 20.0 to 23.1 GPa with an average of 21.2 GPa, and the Poisson's ratio ranges between 0.11 and 0.21 with an average of 0.15. This shows that the mechanical properties of Heituao shale have the characteristics of high elastic modulus and low Poisson's ratio, which is conducive to hydraulic fracturing. In addition, through the observation of the sample morphology after the uniaxial compression tests (Figure 6), it is found that the shale samples are penetrated by cracks perpendicular to the direction of the maximum principal stress, and the crack surface is smooth and straight. The high elastic modulus, low Poisson's ratio, long-straight crack formation and high contents of brittle minerals of the shale samples have a good corresponding relationship to indicate a perfect fracturing potential of the Heituao shale in the study area.

**Table 4.** Mechanical parameters of Heituao shale in the Tadong low uplift.

| Sample No. | Depth (m) | Diameter (mm) | Height (mm) | Young's Modulus (GPa) | Poisson's Ratio |
|---|---|---|---|---|---|
| ML1-7 | 4990 | 25 | 55.3 | 21.864 | 0.12 |
| TD2-3 | 4530 | 25 | 55.64 | 23.144 | 0.11 |
| TD2-4 | 4545 | 25 | 45.7 | 19.996 | 0.21 |
| TD2-6 | 4555 | 25 | 36.12 | 21.324 | 0.15 |

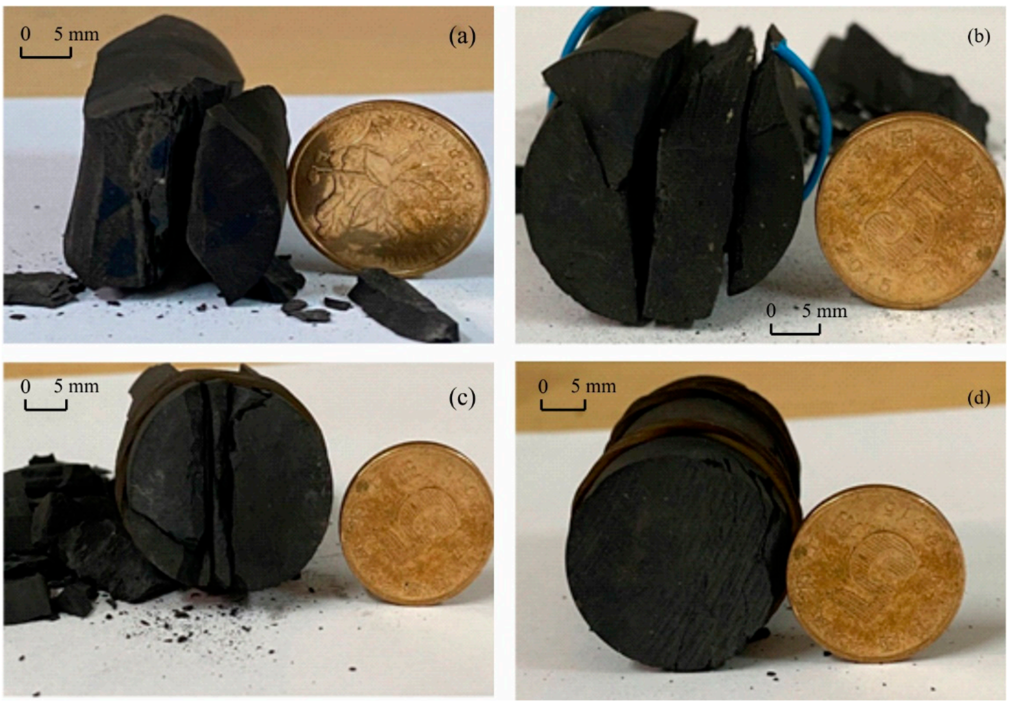


**Figure 6.** The results of uniaxial compression experiments for the Heituao shale samples in Tadong low uplift: (**a**) for sample ML1-7, (**b**) for sample TD2-3, (**c**) for sample TD2-4, (**d**) for sample TD2-6.

## 5. Discussion

Organic geochemical characteristics and mineral compositions are very important for shale gas exploration and development, which determine the exploration potential and development difficulty of shale gas [18–20]. Therefore, it is necessary to conduct a further analysis in order to reveal the abundance, type and maturity of organic matter, as well as the hydraulic fracturing ability of Heituao shale in the study area.

### *5.1. Organic Matter Evaluation*

#### 5.1.1. Organic Matter Abundance

The abundance of organic matter is one of the main factors affecting the hydrocarbon generation intensity of source rocks [33]. Organic matter not only provides the material basis for gas generation, but also serves as the carrier for adsorbed gas which has a close positive correlation with the gas content of shale [1,18]. In addition, the distribution of the TOC versus S2 for the Heituao shale based on a plot [34] was analyzed to reveal the organic matter abundance of Heituao shale in the study area (Figure 7). It indicated that all of the samples can be regarded as having "poor" generative potential, with TOC values ranging from 0.63 to 2.51 wt% (average = 1.22 wt%) and S2 values ranging from 0.08 to 1.37 mg HC/g rock (average = 0.42 mg HC/g rock). Although the TOC values are at a high level, the low S2 values reduce the hydrocarbon generation potential of shale samples, that is to say, the "poor" generative potential mainly results from the S2 values of Heituao shale.

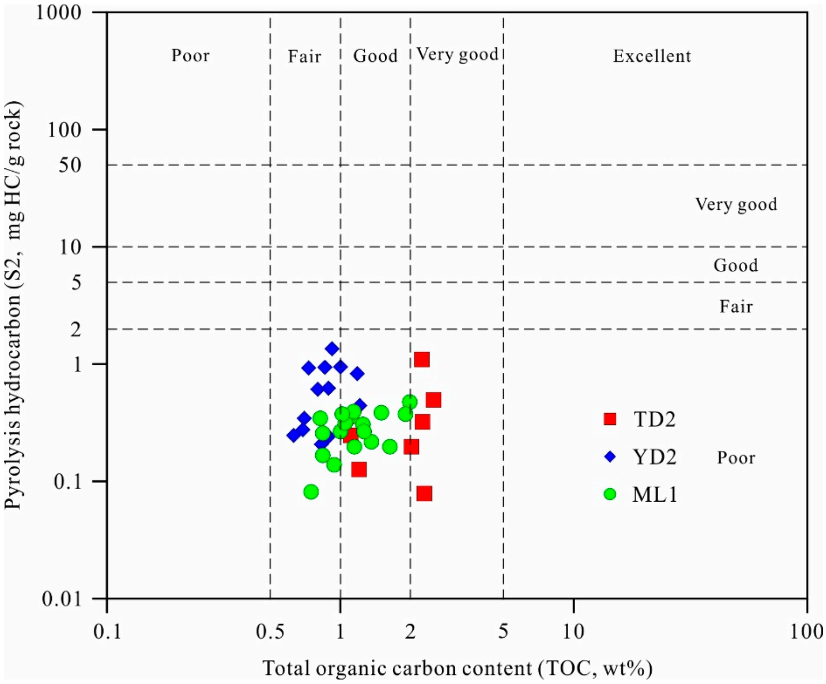


**Figure 7.** The abundance characterization of organic matter for the Heituao shale sample in Tadong low uplift using plot of total organic carbon (TOC) content and pyrolysis hydrocarbon (S2), with the base map after Makeen et al., 2015 [34].

#### 5.1.2. Thermal Maturity

In the process of rock pyrolysis, the maximum pyrolysis temperature corresponding to the highest peak of S2 is the Tmax, which is also a commonly used index to judge the thermal maturity of organic matter [31]. Generally, the Tmax is a very good maturity index for types II and III kerogen and there exists a positive correlation between Tmax and Ro [35,36]. In the process of burial, the organic matter will start to generate hydrocarbon with the increase of thermal evolution degree, while the organic matter with low activation energy will be cracked first, the activation energy of the remaining organic matter is higher, and the energy required for hydrocarbon generation of the same quality organic matter will gradually increase, so the corresponding Tmax for hydrocarbon generation will gradually increase. Previous studies [37,38] have shown that the Tmax values less than 435 °C represent the maturity level of immature; the Tmax values ranging between 435 and 475 °C indicate mature level, among them, 435–455 °C is associated with the oil window and 455–475 °C is the condensate (wet gas) stage; the Tmax values above 475 °C reflect post mature, which is the stage of dry gas.

Moreover, the thermal maturity of organic matter of Heituao shale in the study area was evaluated based on the Tmax values in Figure 8. It indicated that the maturity of Heituao shale varies from immature to post mature, and there exists great difference between different wells which result from different depth (Figure 8a): the shale in well ML1 has experienced post mature with the Tmax values ranging from 477 to 523 °C with an average of 506 °C, that in well YD2 are immature stage maturity with the Tmax values ranging between 382 and 488 °C (average = 437 °C), that in well TD2 are from immature to post mature stage (ranges from 411 to 447 °C, with an average of 428 °C).

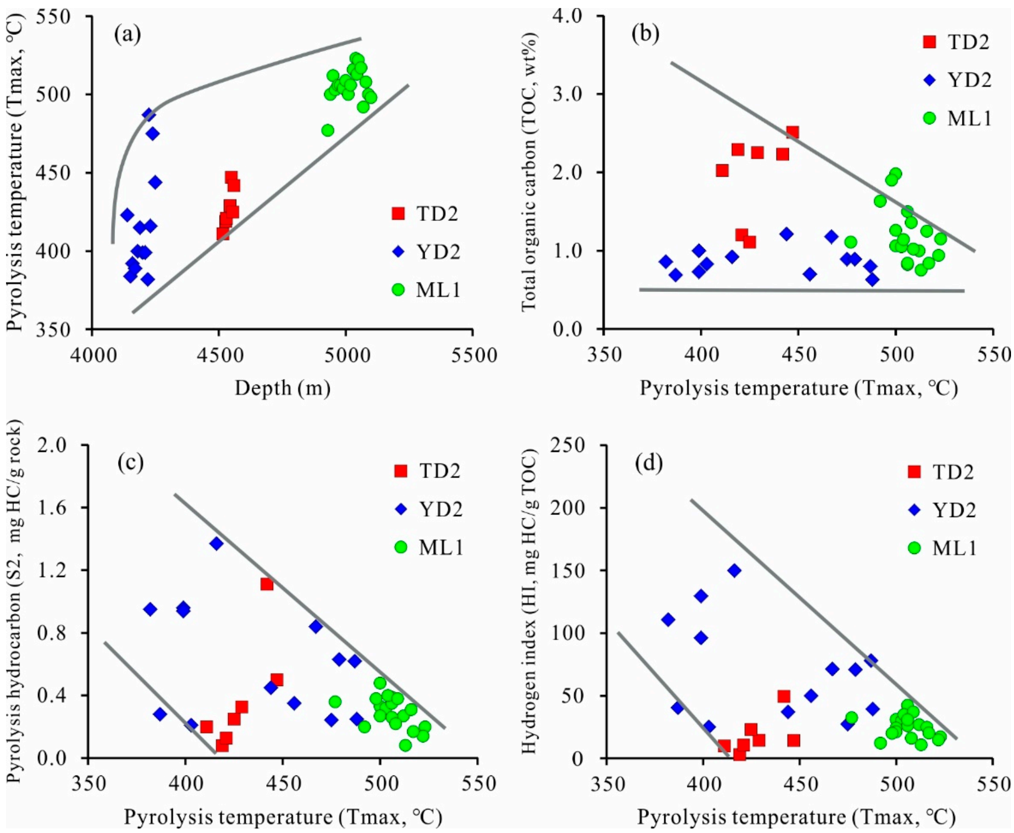


**Figure 8.** The relationship between pyrolysis temperature and (**a**) depth, (**b**) total organic carbon, (**c**) pyrolysis hydrocarbon, (**d**) hydrogen index.

In addition, the thermal maturity of organic matter affects hydrocarbon generation potential of residual organic matter which is indicated in Figure 8b–d. There is a negative correlation between Tmax and TOC, S2 and HI. With the increase of Tmax value, TOC, S2 and HI values show a gradually decreasing trend, and the decreasing degree of S2 and HI is greater than that of TOC. Additionally, with the variation of thermal maturity, the evaluation the abundance and type of organic matter may result in difference. As for the abundance of organic matter, with the maturity of organic matter in shale, a part of hydrocarbon is produced and discharged, which makes the S2 value of the remaining organic matter lower. Therefore, the abundance of organic matter can only indicate the current abundance of the remaining organic matter. Moreover, the higher the maturity is, the more obvious the difference is. Therefore, when evaluating the abundance of past mature organic matter, the lower S2 value results in the lower evaluation result. Relatively speaking, the TOC value changes less with the increase of thermal maturity [39]. Therefore, it is more appropriate to evaluate the abundance of over mature organic matter by a single TOC value.

#### 5.1.3. Organic Matter Type

Due to the great difference of hydrocarbon generation potential of organic matter from different sources and compositions, it is necessary to reveal the type of organic matter of Heituao shale [40]. The type of organic matter can be classified as type I kerogen, type II kerogen, type II-III kerogen, and type III kerogen based on the HI values of shale samples. Previous studies [37,38] have shown that type I kerogen is oil-prone, usually associated with lacustrine environments, with HI values above 600 mg HC/g TOC; type II kerogen is also oil-prone mostly associated with marine environments, with HI values ranging between 300 and 600 mg HC/g TOC; type II-III kerogen is the mixture of types II and III, which is prone to produce oil and gas and associated with the HI values of 200–300 mg HC/g TOC; HI values less than 200 mg HC/g TOC are associated with type III kerogen, which is prone to produce gas and represent the deposition of higher plants. Based on above studies and the plot [37] of HI versus Tmax (Figure 9), it is obvious that all of the shale samples have HI values of less than 200 mg HC/g TOC, showing the type III kerogen type with the characteristic of gas-prone of Heituao shale. However, the results are quite different from the current understanding of the Paleozoic shale [41,42], where only lower organisms exist in its depositional setting, so the organic matter type is unlikely to be classified as type III kerogen which represent the deposition of higher plants. That may be caused by the thermal maturity of organic matter [39,43]. For the type of organic matter, the HI value of past mature organic matter is low, and the classification of organic matter types cannot reflect the original sedimentary environment and materials of organic matter, but only reflect whether organic matter is oil-prone or gas-prone at present. Therefore, it is obvious that organic matter in Heituao shale from Tadong low uplift is gas-prone and has the advantage for shale gas accumulation.

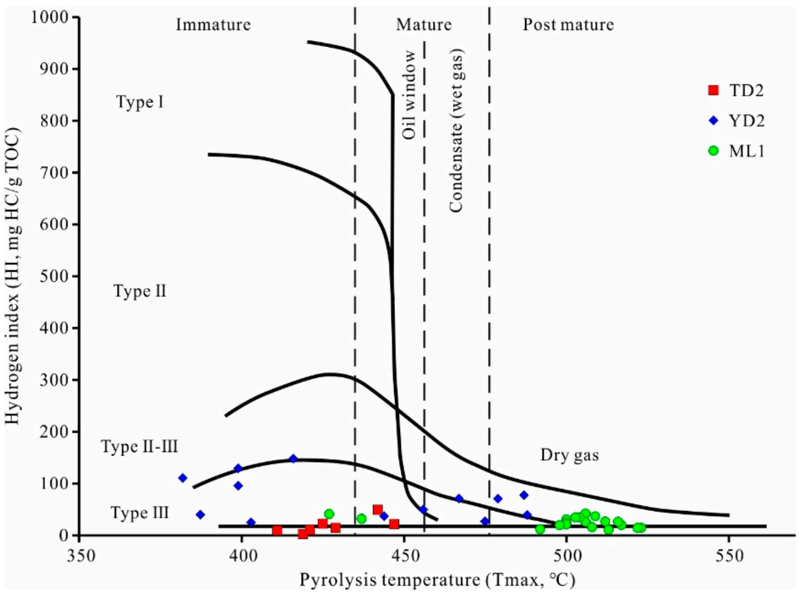


**Figure 9.** The maturity and type of organic matter for the Heituao shale sample in Tadong low uplift plotted on a pyrolysis temperature (Tmax) versus hydrocarbon index (HI), with the base map after Mani et al. 2015 [37].

*5.2. Fracability Evaluation*

Fracability refers to the property that reservoirs can be transformed by hydraulic fracturing to form effective fractures and increase fluid flow capacity, which is a comprehensive reflection of shale geology and reservoir characteristics. Previous studies [44–46] have proved that the main influencing factors on shale fracability are shale brittleness, mineral composition, natural fracture, diagenesis stage, and in-situ stress. In addition, recent studies have shown that diagenetic quartz, not detrital quartz, controls the brittleness of shales [47,48]. At present, the current methods to evaluate shale fracability are mainly mineral composition method and rock mechanics method, and the brittleness index (BI) based on mineral composition method has been proved to be a comprehensive and applicable method to evaluate the fracability compared with that based on rock mechanics method [49,50], which is widely used [51] with the Equation (1).

$$\mathrm{BI} = \frac{Vquatrtz + Vdolomite}{Vquartz + Vdolomite + Vclay + Vcalcite + Vtoc} \tag{1}$$

where, BI is the brittleness index, 0~1; *Vquatrtz* is the content of diagenetic quartz, %; *Vdolomite* is the content of dolomite, %; *Vclay* is the content of clay minerals, %; *Vcalcite* is the calcite content, %; *Vtoc* is the TOC content, %.

Obviously, the larger the BI value, the better the fracturing effect of shale. The BI values of the studied shale samples are determined based on Equation (1), which are shown in Table 2. From the result we can see that the BI values range between 0.28 and 0.99 with an average of 0.85, which is higher than 0.5 and other shales, indicating the good fracturing potential of Heituao shale in the study area.

In order to ensure the accuracy of BI value, it is necessary to compare and verify the results by the fracability evaluation based on rock mechanics method. At present, the brittleness average (BA) value is used with the Equation (2) to evaluate shale compressibility [31].

$$\mathrm{BA} = \left(\frac{E - Emin}{Emax - Emin} + \frac{Vmax - V}{Vmax - Vmin}\right)/2 \tag{2}$$

where, BA is the brittleness average, 0~1; *E* is the Young's modulus of sample, GPa; *Emax* and *Emin* are the maximum and minimum Young's modulus, respectively, of the formation in the vertical direction, GPa; *V* is the Poisson's ratio of sample, *Vmax* and *Vmin* are the maximum and minimum Poisson's ratio, respectively, of the formation in the vertical direction.

However, it is difficult to obtain the maximum and minimum Young's modulus and Poisson ratio of the formation in vertical direction in the study area, so the above method is not applicable in the study area.

Considering the difference of micromechanical properties [52] between different minerals and the relationship between mineral composition and brittleness index, an improved fracability evaluation model of Equation (3) is obtained based on Equations (1) and (2):

$$\mathrm{BM} = \frac{EM - EMmin}{EMmax - EMmin} \tag{3}$$

$$\mathrm{EM} = \frac{Vquatrtz \times Equartz + Vdolomite \times Edolomite + Vclay \times Eclay + Vcalcite \times Eclay + Vtoc \times Etoc}{Vquartz + Vdolomite + Vclay + Vcalcite + Vtoc} \tag{4}$$

where, BM is the brittleness of minerals, 0~1; EM is the average Young's modulus of minerals in sample, GPa; *EMmax* and *EMmin* are the maximum and minimum Young's modulus, respectively, of minerals, GPa; *Equartz* is the Young's modulus of quartz, GPa; *Edolomite* is the Young's modulus of dolomite, GPa; *Eclay* is the Young's modulus of clay minerals, GPa; *Ecalcite* is the Young's modulus of calcite, GPa; *Etoc* is the Young's modulus of TOC, GPa. The Young's modulus of minerals can be obtained by nanoindentation [53] and atomic force microscopy [54] and related data used in this study is shown in Table 5, from that we can see *EMmax* and *EMmin* are the Young's modulus of dolomite and clay, respectively, of Heituao shale in the study area, thus Equation (3) can be transformed into Equation (5):

$$\mathrm{BM} = \frac{EM - Eclay}{Equartz - Eclay} \tag{5}$$

**Table 5.** Young's modulus of different minerals and organic matter based on previous studies.

| Minerals | TOC | Quartz | Clay | Dolomite | Calcite |
|---|---|---|---|---|---|
| Density (g/cm$^3$) | 1.23 | 2.65 | 2.7 | 2.84 | 2.71 |
| Young's modulus (GPa) | 10.5 | 87.2 | 18.5 | 116.6 | 84.3 |
| Sources | [55] | [55] | [55] | [56] | [56] |

The BM values of Heituao shale samples are evaluated based on Equation (5), which ranges between 0.26 and 0.83 with an average of 0.67, indicating the good fracturing potential of Heituao shale in the study area.

In addition, by comparing BI and BM values (Figure 10), it is found that BI value is slightly higher than BM value, and there is a certain positive correlation between them. Moreover, it shows that BI and BM values have a good positive correlation with the Young's modulus, and a good negative correlation with the Poisson's ratio of shale samples. With the increase of Young's modulus and the decrease of Poisson's ratio, BI and BM values show an increasing trend, which shows the feasibility and accuracy of evaluating the fracability of Heituao shale in the study area through these two parameters.

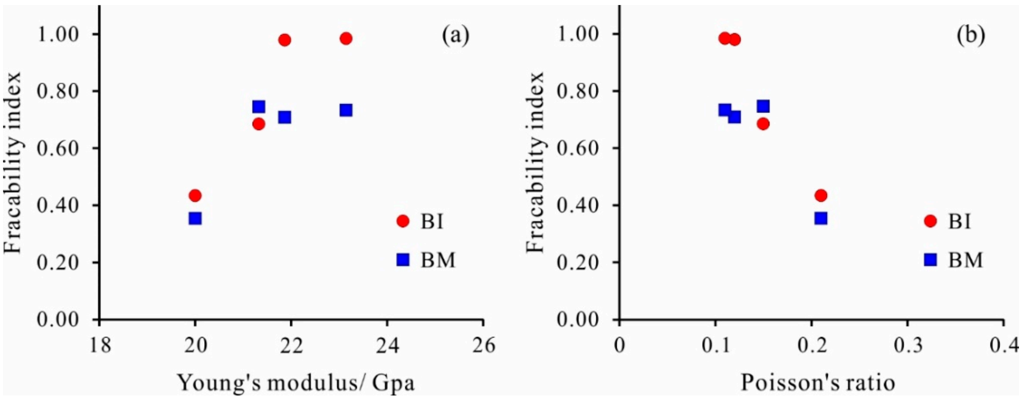


**Figure 10.** The relationship of Heituao shale samples in Tadong low uplift between mechanical parameters and brittleness parameters: (**a**) relationship between brittleness index (BI), brittle mineral (BM), and Young's modulus; (**b**) relationship between brittleness index (BI), brittle mineral (BM), and Poisson's ratio.

### *5.3. Shale Gas Production Potential in Tadong Low Uplift*

Heituao shale has great differences compared with others [41,42,57]. Firstly, in terms of organic geochemical characteristics, its high Tmax value reveals a high degree of evolution. In this high degree of background, TOC content is at a general level, and S2 value is small. Although the current shale geochemical parameters are generally fair or poor, it also shows that Heituao formation shale in the study area has generated a lot of hydrocarbons. In addition, Heituao shale has the characteristics of ultra-low porosity and permeability, which purport the necessity of hydraulic fracturing before shale gas exploitation. In terms of mineral composition, Heituao shale shows ultra-high quartz content, indicating its high fracability and good hydraulic fracturing effect, and the uniaxial compression test results further reveal the characteristics of good fracturing performance. At present, the important factor hindering the development of Heituao formation shale gas in the study area is the depth with almost 4000–5000 m, which is unattainable for the current shale gas production technology. However, with the improvement of technology and methodology, the Heituao shale gas in Tadong low uplift will become possible soon or later.

## 6. Conclusions

The geochemical, mineralogical and mechanical characteristics of Heituao shale in Tadong low uplift were analyzed, together with the development potential of shale gas. The following conclusions can be obtained:

1. The organic matter of Heituao shale in the study area show poor abundance and type III kerogen type, which are mainly caused by the post mature organic matter; quartz is the main mineral component in Heituao shale samples, and its Young's modulus is high and Poisson's ratio is low.
2. Organic matter of Heituao shale in the study area has experienced post mature and at the stage of dry gas, indicating the large hydrocarbons generation and occurrence. In addition, Heituao shale shows ultra-high quartz content, indicating its high fracability and good hydraulic fracturing effect.
3. The Heituao shale is characterized by large depth (4100–5100 m), large thickness (50–200 m), wide and stable distribution in the study area. The depth of shale is a challenge for current shale gas development, but Heituao shale gas in Tadong low uplift will attract interest with the improvement of technology and methodology.

**Author Contributions:** Conceptualization, S.Z. and Y.L.; methodology, S.Z.; validation, S.Z., and X.G.; formal analysis, S.Z.; investigation, S.Z.; resources, H.L. and Z.X.; data curation, H.L. and Z.X.; writing—original draft preparation, S.Z.; writing—review and editing, Y.L.; visualization, X.G.; supervision, Y.W.; project administration, Y.W.; funding acquisition, Y.W. All authors have read and agreed to the published version of the manuscript.

**Funding:** This study was funded by the National Science Foundation of China (Grant No. 42072194), the Major National Science and Technology Project of China (No. 2016ZX05066001-002; 2017ZX05064-003-001).

**Data Availability Statement:** The data presented in this study are available in the article.

**Acknowledgments:** We thank the Research Institute of Petroleum Exploration and Development and Tarim Oil Co. of CNPC for providing testing samples, and our colleagues for the beneficial suggestion.

**Conflicts of Interest:** We declare that we have no financial and personal relationships with other people or organizations that can inappropriately influence our work, there is no professional or other personal interest of any nature or kind in any product, service and/or company that could be construed as influencing the position presented in, or the review of, the manuscript entitled.

## References

1. Zou, C.N.; Zhu, R.K.; Chen, Z.Q.; Ogg, J.G.; Wu, S.T.; Dong, D.Z.; Qiu, Z.; Wang, Y.M.; Wang, L.; Lin, S.H.; et al. Organic-matter-rich shales of China. *Earth Sci. Rev.* **2019**, *189*, 51–78. [CrossRef]
2. Li, Y.; Tang, D.Z.; Wu, P.; Niu, X.L.; Wang, K.; Qiao, P.; Wang, Z.S. Continuous unconventional natural gas accumulations of Carboniferous-Permian coal-bearing strata in the Linxing area, northeastern Ordos basin, China. *J. Nat. Gas Sci. Eng.* **2016**, *36*, 314–327. [CrossRef]
3. Montgomery, S.L.; Jarvie, D.M.; Bowker, K.A.; Pollastro, R.M. Mississippian Barnett Shale, Fort Worth basin, north-central texas: Gas-shale play with multi-trillion cubic foot potential. *AAPG Bull.* **2005**, *89*, 155–175. [CrossRef]
4. Gasparik, M.; Bertier, P.; Gensterblum, Y.; Ghanizadeh, A.; Krooss, B.M.; Littke, R. Geological controls on the methane storage capacity in organic-rich shales. *Int. J. Coal. Geol.* **2013**, *123*, 34–51. [CrossRef]
5. Kinley, T.J.; Cook, L.W.; Breyer, J.A.; Jarvie, D.M.; Busbey, A.B. Hydrocarbon potential of the Barnett Shale (Mississippian), Delaware Basin, west Texas and southeastern New Mexico. *AAPG Bull.* **2008**, *92*, 962–991. [CrossRef]
6. Chen, S.B.; Zhu, Y.M.; Wang, H.Y.; Liu, H.L.; Wei, W.; Fang, J.H. Shale gas reservoir characterisation: A typical case in the southern Sichuan Basin of China. *Energy* **2011**, *36*, 6609–6616. [CrossRef]
7. Guo, T.L.; Zhang, H.R. Formation and enrichment mode of Jiaoshiba shale gas field, Sichuan Basin. *Pet. Explor. Dev.* **2014**, *41*, 31–40. [CrossRef]
8. Hao, F.; Zou, H.Y.; Lu, Y.C. Mechanisms of shale gas storage: Implications for shale gas exploration in China. *AAPG Bull.* **2013**, *97*, 1325–1346. [CrossRef]

9. Li, Y.; Wang, Z.S.; Pan, Z.J.; Niu, X.L.; Yu, Y.; Meng, S.Z. Pore structure and its fractal dimensions of transitional shale: A cross-section from east margin of the Ordos Basin, China. *Fuel* **2019**, *241*, 417–431. [CrossRef]
10. Guo, M.Y.; Lu, X.; Nielsen, C.P.; McElroy, M.B.; Shi, W.R.; Chen, Y.T.; Xu, Y. Prospects for shale gas production in China: Implications for water demand. *Renew. Sust. Energy Rev.* **2016**, *66*, 742–750. [CrossRef]
11. Pang, X.Q.; Jia, C.Z.; Chen, J.Q.; Li, M.W.; Wang, W.Y.; Hu, Q.H.; Guo, Y.C.; Chen, Z.X.; Peng, J.W.; Liu, K.Y.; et al. A unified model for the formation and distribution of both conventional and unconventional hydrocarbon reservoirs. *Geosci. Front.* **2020**, *12*, 695–711. [CrossRef]
12. Liu, X.P.; Jin, Z.J.; Bai, G.P.; Liu, J.; Guan, M.; Pan, Q.H.; Li, T. A comparative study of salient petroleum features of the Proterozoic-Lower Paleozoic succession in major petroliferous basins in the world. *Energy Explor. Exploit.* **2017**, *35*, 54–74. [CrossRef]
13. Cai, X.Y.; Wang, Y. The formation and distribution of the marine hydrocarbon source rock in the Tarim basin, NW China. *Acta Geol. Sin. Engl. Ed.* **2008**, *82*, 509–519.
14. Gao, Z.Y.; Zhang, S.C.; Zhang, X.Y.; Zhu, R.K. Relations between spatial distribution and sequence types of the Cambrian-Ordovician marine source rocks in Tarim Basin. *Chin. Sci. Bull.* **2007**, *52*, 92–102. [CrossRef]
15. Liu, D.M.; Tu, J.Q.; Jin, K.L. Organic petrology of potential source rocks in the Tarim Basin, NW China. *J. Pet. Geol.* **2003**, *26*, 105–124. [CrossRef]
16. Zheng, Y.J.; Liao, Y.H.; Wang, Y.P.; Xiong, Y.Q.; Peng, P.A. Organic geochemical characteristics, mineralogy, petrophysical properties, and shale gas prospects of the Wufeng-Longmaxi shales in Sanquan Town of the Nanchuan District, Chongqing. *AAPG Bull.* **2018**, *102*, 2239–2265. [CrossRef]
17. Guo, X.S.; Li, Y.P.; Borjigen, T.; Wang, Q.; Yuan, T.; Shen, B.J.; Ma, Z.L.; Wei, F.B. Hydrocarbon generation and storage mechanisms of deep-water shelf shales of Ordovician Wufeng Formation-Silurian Longmaxi Formation in Sichuan Basin, China. *Pet. Explor. Dev.* **2020**, *47*, 204–213. [CrossRef]
18. Guo, W.; Hu, Z.M.; Zhang, X.W.; Yu, R.Z.; Wang, L. Shale gas adsorption and desorption characteristics and its effects on shale permeability. *Energy Explor. Exploit.* **2017**, *35*, 463–481. [CrossRef]
19. Yao, X.L.; Wang, Y.P. Assessing shale gas resources of Wufeng-Longmaxi shale (O3w-S1l) in Jiaoshiba area, SE Sichuan (China) using Petromod II: Gas generation and adsorption. *Pet. Sci. Technol.* **2016**, *34*, 1008–1015. [CrossRef]
20. Ma, C.F.; Dong, C.M.; Lin, C.Y.; Elsworth, D.; Luan, G.Q.; Sun, X.L.; Liu, X.C. Influencing factors and fracability of lacustrine shale oil reservoirs. *Mar. Pet. Geol.* **2019**, *110*, 463–471. [CrossRef]
21. Feng, R.H.; Zhang, Y.H.; Rezagholilou, A.; Roshan, H.; Sarmadivaleh, M. Brittleness Index: From Conventional to Hydraulic Fracturing Energy Model. *Rock Mech. Rock Eng.* **2020**, *53*, 739–753. [CrossRef]
22. Zhu, G.Y.; Milkov, A.V.; Li, J.F.; Xue, N.; Chen, Y.Q.; Hu, J.F.; Li, T.T.; Zhang, Z.Y.; Chen, Z.Y. Deepest oil in Asia: Characteristics of petroleum system in the Tarim basin, China. *J. Pet. Sci. Eng.* **2021**, *199*, 108246. [CrossRef]
23. Li, J.Z.; Tao, X.W.; Bai, B.; Huang, S.P.; Jiang, Q.C.; Zhao, Z.Y.; Chen, Y.Y.; Ma, D.B.; Zhang, L.P.; Li, N.X.; et al. Geological conditions, reservoir evolution and favorable exploration directions of marine ultra-deep oil and gas in China. *Pet. Explor. Dev.* **2021**, *48*, 60–79. [CrossRef]
24. Hu, G.Y.; Li, J.; Cui, H.Y.; Ran, Q.G.; Zhang, L.; Wang, X.B.; Wang, Y.F. The generation and its sealing condition of natural gas in the Tadong area. *Sci. China Ser. D.* **2009**, *52*, 96–105. [CrossRef]
25. He, B.Z.; Xu, Z.Q.; Rao, C.L.; Li, H.B.; Cai, Z.H. Tectonic unconformities and their forming: Implication for hydrocarbon accumulations in Tarim basin. *Acta Petrol. Sin.* **2011**, *27*, 253–265.
26. Liu, H.; Lin, C.S.; Guo, R.B.; Zhu, M.; Cui, Y.Q. Characteristics of the Paleozoic slope break system and its control on stratigraphic-lithologic traps: An example from the Tarim Basin, western China. *J. Palaegeogr.* **2015**, *4*, 284–304. [CrossRef]
27. Lin, C.S.; Li, S.T.; Liu, J.Y.; Qian, Y.X.; Luo, H.; Chen, J.Q.; Peng, L.; Rui, Z.F. Tectonic framework and paleogeographic evolution of the Tarim basin during the Paleozoic major evolutionary stages. *Acta Petrol. Sin.* **2011**, *27*, 210–218.
28. Chen, Y.Q.; Zhang, Y.Q.; Wu, Y.S.; Zhou, P.; Li, K.K.; Wang, X.X. Discovery of SPICE and carbon isotope stratigraphic correlation of the Cambrian Furongian Series in Tarim Craton, NW China. *China-Earth Sci.* **2020**, *63*, 1330–1338. [CrossRef]
29. Glaser, K.S.; Miller, C.K.; Johnson, G.M.; Kleinberg, R.L.; Pennington, W.D. Seeking the sweet Spot: Reservoir and completion quality in organic shales. *Oilfield Rev.* **2014**, *25*, 16–29.
30. Rimstidt, J.D.; Chermak, J.A.; Schreiber, M.E. Processes that control mineral and element abundances in shales. *Earth Sci. Rev.* **2017**, *171*, 383–399. [CrossRef]
31. Kumar, S.; Das, S.; Bastia, R.; Ojha, K. Mineralogical and morphological characterization of Older Cambay Shale from North Cambay Basin, India: Implication for shale oil/gas development. *Mar. Pet. Geol.* **2018**, *97*, 339–354. [CrossRef]
32. Laubach, S.E.; Olson, J.E.; Gross, M.R. Mechanical and fracture stratigraphy. *AAPG Bull.* **2009**, *93*, 1413–1426. [CrossRef]
33. Van Krevelin, D.W. *Coal: Typology, Chemistry, Physics, Constitution*; Elsevier Science: Amsterdam, The Netherlands, 1961.
34. Makeen, Y.M.; Abdullah, W.H.; Hakimi, M.H.; Mustapha, K.A. Source rock characteristics of the Lower Cretaceous Abu Gabra Formation in the Muglad Basin, Sudan, and its relevance to oil generation studies. *Mar. Pet. Geol.* **2015**, *59*, 505–516. [CrossRef]
35. Peters, K.E.; Cassa, M.R. Applied source rock geochemistry. In *The Petroleum System-From Source to Trap*; AAPG Memoir 60: Tulsa, OK, USA, 1994.
36. Jarvie, D.M.; Claxton, B.L.; Henk, F.; Breyer, J.T. Oil and shale gas from the Barnett Shale, Ft. In *Worth Basin, Texas*; AAPG Annual Meeting Program; AAPG: Denver, CO, USA, 2001.

37. Mani, D.; Patil, D.J.; Dayal, A.M.; Prasad, B.N. Thermal maturity, source rock potential and kinetics of hydrocarbon generation in Permian shales from the Damodar Valley basin, Eastern India. *Mar. Pet. Geol.* **2015**, *66*, 1056–1072. [CrossRef]
38. Goodarzi, F.; Haeri-Ardakani, O.; Gentzis, T.; Pedersen, P.K. Organic petrology and geochemistry of Tournaisian-age Albert Formation oil shales, New Brunswick, Canada. *Int. J. Coal. Geol.* **2019**, *205*, 43–57. [CrossRef]
39. Tao, S.; Wang, Y.B.; Tang, D.Z.; Xu, H. Hydrocarbon-generation in Cambrian-Silurian high- to over- mature source rocks, middle and upper Yangtze region, China. *Energy Explor. Exploit.* **2012**, *30*, 19–42. [CrossRef]
40. Nixon, R.P. Oil source beds in cretaceous Mowry shale of North-western Interior United States. *Am. Assoc. Pet. Geol. Bull.* **1973**, *57*, 136–161.
41. Li, D.L.; Li, R.X.; Zhao, D.; Xu, F. Petrography and Organic Geochemistry Characterizations of Lower Paleozoic Organic-Rich Shale in the Northwestern Upper Yangtze Plate: Niutitang Formation and Longmaxi Formation, Dabashan Foreland Belt. *Minerals* **2018**, *8*, 439. [CrossRef]
42. Kosakowski, P.; Kotarba, M.J.; Piestrzynski, A.; Shogenova, A.; Wieclaw, D. Petroleum source rock evaluation of the Alum and Dictyonema Shales (Upper Cambrian-Lower Ordovician) in the Baltic Basin and Podlasie Depression (eastern Poland). *Int. J. Earth Sci.* **2017**, *106*, 743–761. [CrossRef]
43. Gao, J.L.; Ni, Y.Y.; Li, W.; Yuan, Y.L. Pyrolysis of coal measure source rocks at highly to over mature stage and its geological implications. *Petroleum Explor. Dev.* **2020**, *47*, 773–780. [CrossRef]
44. Ye, Y.P.; Tang, S.H.; Xi, Z.D. Brittleness Evaluation in Shale Gas Reservoirs and Its Influence on Fracability. *Energies* **2020**, *13*, 388. [CrossRef]
45. Lizcano-Hernandez, E.G.; Nicolas-Lopez, R.; Valdiviezo-Mijangos, O.C.; Melendez-Martinez, J. Estimation of brittleness indices for pay zone determination in a shale-gas reservoir by using elastic properties obtained from micromechanics. *J. Geophys. Eng.* **2018**, *15*, 307–314. [CrossRef]
46. Xia, Y.J.; Zhou, H.; Zhang, C.Q.; He, S.H.; Gao, Y.; Wang, P. The evaluation of rock brittleness and its application: A review study. *Eur. J. Environ. Civ. Eng.* **2019**, *45*, 139–145. [CrossRef]
47. Liu, B.; Schieber, J.; Mastalerz, M.; Teng, J. Variability of rock mechanical properties in the sequence stratigraphic context of the Upper Devonian New Albany Shale, Illinois Basin. *Mar. Pet. Geol.* **2020**, *112*, 104068. [CrossRef]
48. Xi, Z.D.; Tang, S.H.; Zhang, S.H.; Yi, Y.X.; Dang, F.; Ye, Y.P. Characterization of quartz in the Wufeng Formation in northwest Hunan Province, south China and its implications for reservoir quality. *J. Pet. Sci. Eng.* **2019**, *179*, 979–996. [CrossRef]
49. Moghadam, A.; Harris, N.B.; Ayranci, K.; Gomez, J.S.; Angulo, N.A.; Chalaturnyk, R. Brittleness in the Devonian Horn River shale, British Columbia, Canada. *J. Nat. Gas Sci. Eng.* **2018**, *62*, 247–258. [CrossRef]
50. Shimizu, H.; Ito, T.; Tamagawa, T.; Tezuka, K. A study of the effect of brittleness on hydraulic fracture complexity using a flow-coupled discrete element method. *J. Pet. Sci. Eng.* **2018**, *160*, 372–383. [CrossRef]
51. Wang, F.P.; Gale, J.F.W. Screening criteria for shale-gas systems. *Gulf Coast Assoc. Geol. Soc. Trans.* **2009**, *59*, 779–793.
52. Li, Y.; Yang, J.H.; Pan, Z.J.; Tong, W.S. Nanoscale pore structure and mechanical property analysis of coal: An insight combining AFM and SEM images. *Fuel* **2020**, *260*, 116352. [CrossRef]
53. Li, C.X.; Ostadhassan, M.; Gentzis, T.; Kong, L.Y.; Carvajal-Ortiz, H.; Bubach, B. Nanomechanical characterization of organic matter in the Bakken formation by microscopy-based method. *Mar. Pet. Geol.* **2018**, *96*, 128–138. [CrossRef]
54. Zhao, S.H.; Li, Y.; Wang, Y.B.; Ma, Z.T.; Huang, X.Q. Quantitative study on coal and shale pore structure and surface roughness based on atomic force microscopy and image processing. *Fuel* **2019**, *244*, 78–90. [CrossRef]
55. Zhao, J.L.; Zhang, D.X.; Wu, T.H.; Tang, H.Y.; Xuan, Q.H.; Jiang, Z.; Dai, C. Multiscale Approach for Mechanical Characterization of Organic-Rich Shale and Its Application. *Int. J. Geomech.* **2019**, *19*, 04018180. [CrossRef]
56. Wang, Z.J.; Wang, H.; Cates, M.E. Effective elastic properties of solid clays. *Geophysics* **2001**, *66*, 428–440. [CrossRef]
57. Tuo, J.C.; Wu, C.J.; Zhang, M.F. Organic matter properties and shale gas potential of Paleozoic shales in Sichuan Basin, China. *J. Nat. Gas Sci. Eng.* **2016**, *28*, 434–446. [CrossRef]